CrystEngComm

PAPER

View Article Online
View Journal | View Issue

Check for updates

Cite this: *CrystEngComm*, 2024, **26**, 4579

Dye adsorption performance of an anionic Cd^{2+} MOF material based on semi-rigid hexacarboxylic acid†

Yuxuan Xiong,[a] Dan-Dan Li,[a] Jie-Hui Yu *[a] and Qingfeng Yang *[b]

Received 14th April 2024,
Accepted 22nd July 2024

DOI: 10.1039/d4ce00362d

rsc.li/crystengcomm

We have selected a semi-rigid hexacarboxylic acid ligand H_6L enriched with oxygen-active sites with Cd^{2+} salt, successfully synthesising a 3-D anionic material MOF-1 ($[(CH_3)_2NH_2]_2[Cd_2L]\cdot 3DMA\cdot 2H_2O$, H_6L = 5,5′,5″-(benzene-1,3,5-triyltris(oxy))triisophthalic acid). The structure of this carboxylic acid ligand is triangular in shape, which contributes to the formation of the 3-D framework structure, and its semi-rigidity facilitates entry of dye molecules by slightly adjusting the pore size. The larger pore size of MOF-1 is 1.45 nm × 0.86 nm. The oxygen spacer groups are uniformly distributed throughout the framework, promoting the adsorption of MOF-1 for dyes. Based on these factors, there is a significant advantage in that the anionic material MOF-1 containing $[(CH_3)_2NH_2]^+$ selectively adsorbs cationic organic dyes from aqueous contaminants for recycling. It was discovered that the adsorption process' equilibrium and kinetics followed the Langmuir isothermal model and pseudo-secondary kinetics, respectively. And we measured the adsorption rate of MOF-1′ on MB^+ to be 1.77×10^{-3} g mg^{-1} min^{-1}. Its relatively high capacity is *ca.* 1220 mg g^{-1}. After five cycles of adsorption and desorption, the dye adsorption performance was reduced to *ca.* 80% and the framework stability remained well.

Published on 23 July 2024. Downloaded on 11/19/2024 3:34:02 PM.

Introduction

Dyes are categorized into synthetic and natural dyes. Synthetic dyes are widely used in industrial production due to better sustainability and a wide range of coloring types.[1] However, synthetic dyes do not degrade over time and are carcinogenic to humans due to prolonged exposure. Because of their toxicity, synthetic dyes have damaged the equilibrium and integrity of ecosystems in recent years, endangering both human health and the environment.[2–4] This has led to a surge of interest in the treatment of dye wastewater. Compared with other dye treatment technologies such as solid phase extraction,[5,6] photocatalysis,[7–9] membrane separation[10–12] and electrolysis,[13–15] adsorption is considered to be one of the most popular methods to effectively remove pollutants due to its high efficiency and simplicity of operation.[16–20] The ideal catalyst should have a large specific surface area and excellent stability for effectively adsorbing dyes. From the beginning, the application of traditional adsorbents has been limited due to poor adsorption capacity, low adsorption rate, and insufficient functional modulation.[21,22] Metal oxide materials and zero-valent iron materials have been limited due to poor chemical stability.[23,24] Carbon-based nanomaterials have been limited due to high cost of preparation, complexity of the preparation process, and low selectivity.[25] In recent years, MOFs have been continuously developed since they were proposed by Yaghi in 1995,[26] and have made excellent contributions to catalysis,[27–29] dyestuffs,[30–32] and adsorption[33] due to their properties such as high porosity, high stability, and tunability. MOF-based micro/nanomaterials have shown excellent water purification capabilities and have been widely used as adsorbents or catalysts for environmental remediation.[34,35] MOFs can be applied directly or utilised as precursors or composites because of the variety of types and synthesis techniques of MOF-based materials. The use of different metal centers helps to predict the structure of the synthesized MOFs, for example, the metal center Cd and polycarboxylic acid organic ligands are prone to form two or even higher

[a] *College of Chemistry, and State Key Laboratory of Inorganic Synthesis and Preparative Chemistry, Jilin University, Changchun, Jilin, 130012, P. R. China. E-mail: jhyu@jlu.edu.cn*

[b] *State Key Laboratory Cultivation Base of Natural Gas Conversion, College of Chemistry and Chemical Engineering, Ningxia University, Yinchuan, 750021, P. R. China. E-mail: yangqf@nxu.edu.cn*

† Electronic supplementary information (ESI) available: Materials and physical measurements, molecular structures, crystal data, adsorption capacity and kinetic parameters of MB^+ for various materials, crystal structure, IR spectra, PXRD patterns, TG curve, comparison of dye desorption in acetonitrile solution containing saturated NaCl and pure acetonitrile solution, and calculation formula for dyes. (**PDF**). CCDC 2059712. For ESI and crystallographic data in CIF or other electronic format see DOI: **https://doi.org/10.1039/d4ce00362d**

Published on 23 July 2024. Downloaded on 11/19/2024 3:34:02 PM.

dimensional framework materials.[36] The functionalisation of pores in frameworks depends more on the choice of ligands. On the one hand, organic ligands' functional groups, which are distributed evenly throughout the MOF materials' skeleton as functionalization sites, can interact with dyes that contain unsaturated groups, like azo groups, enhancing the MOF materials' adsorption capacity.[37] On the other hand, the shape, stiffness, and flexibility of ligands improve performance through partially affecting the stability and multi-dimensionality of MOFs. In our previous research, we designed and selected organic ligands containing N atoms and introduced them into the backbone structure of MOFs. It can significantly improve the adsorption performance of dye molecules through the weak interaction of N atoms with adsorbates.[38] Therefore, we hypothesized that the introduction of oxygen atoms may have the same effect. Based on the literature survey, Wang Yao *et al.* synthesized two MOF materials through two hetero-structured polymeric aromatic carboxylic acid ligands containing methoxy groups with cupric ions. The methoxy groups of the two MOFs are believed to effectively enhance the attraction between the framework with acetylene and carbon dioxide molecules which are easily polarized. In this way, the MOFs can be used to improve the adsorption performance and selectivity to gases.[39] Dongjie Bai *et al.* synthesized four new 3-D lanthanide MOFs using cyclic triphosphonitrile-functionalized hexacarboxylate derivatives with different substituents (methoxy, chloro, bromo, and methyl groups). The N_2 adsorption and desorption studies showed that only the methoxy-modified Ln-MOF-ZJNU-63 exhibits permanent porosity after activation among these Ln-MOFs.[40] Therefore, the introduction of oxygen atoms into the framework may be able to promote the adsorption capacity of MOFs for dyes through weak molecular interactions such as electrostatic interaction, hydrogen bonding, and van der Waals interaction.

In this paper, we chose an organic aromatic polycarboxylic acid ligand with oxygen spacer groups. This triangular ligand with divalent metal cadmium helps to form a high-dimensional framework structure. In this way, the MOF can provide larger cavities to accommodate space for guest molecules. Meanwhile, oxygen atoms on the ligand are introduced into the framework to interact with dyes. Moreover, this semi-rigid ligand can facilitate the entry of dye molecules through slightly tuning the pore size. Therefore, the adsorption performance of MOFs for dyes may be significantly improved.

As predicted, we successfully combined this ligand with divalent cadmium ions to synthesize a 3-D coordination polymer material MOF-1 ($[(CH_2)_2NH_2]_2[Cd_2(L)]\cdot 3DMA\cdot 2H_2O$, H_6L = 5,5′,5″-(benzene-1,3,5-triyltris(oxy))triisophthalic acid). MOF-1 has a 3-D anionic structure and $[(CH_3)_2NH_2]^+$ is in its pores for balancing the charge of the anionic skeleton, which is a strong driving force for adsorption of dyes. Based on the above advantages, we revealed the dye adsorption mechanism of MOF-1, investigated and analyzed its adsorption kinetics.

Experimental section

Synthesis of MOF-1

$[(CH_3)_2NH_2]_2[Cd_2(L)]\cdot 3DMA\cdot 2H_2O$ (MOF-1). MOF-1 was synthesized through the solvothermal method. H_6L (0.1 mmol, 62 mg), $CdCl_2\cdot 2.5H_2O$ (46 mg, 0.2 mmol) and 2.5 mL mixed solution of DMA (DMA = *N*,*N*-dimethylacetamide) and H_2O (4 : 1 in volume) were put in a 25 mL Teflon-lined stainless vessel. The pH of the solution was adjusted to 4 with concentrated nitric acid. After being stirred for 30 min, the system was heated at 105 °C for 72 h. Then, it was cooled down to 30 °C at a rate of 5 °C h^{-1}. Pale yellow columnar crystals were obtained and washed with DMA and H_2O (yield: about 39% based on Cd^{2+}). Anal. calculated for $C_{46}H_{59}N_5O_{20}$-Cd_2. MOF-1: C 45.04, H 4.848, N 5.71%; found: C, 44.93, H, 4.615, N, 5.76%. IR (KBr, cm^{-1}): 3422 (w), 3078 (w), 2933 (w), 2799 (w), 2478 (w), 1618 (s), 1564 (s), 1447 (m), 1400 (s), 1369 (s), 1246 (s), 1138 (s), 1021 (s), 932 (w), 854 (w), 781 (s), 730 (s), 592 (w), 432 (w).

Synthesis of MOF-1′

MOF-1′ was obtained by activation in a vacuum drying oven at a temperature of 80 °C for 12 h.

X-ray crystallography

The crystal data of MOF-1 are presented in Table S1.† The diffraction data were obtained by using a Rigaku *R*-AXIS RAPID CCD diffractometer equipped with a MoKα radiation source (λ = 0.71073 Å). The structure of MOF-1 was analyzed by the SHELXT program using direct methods. In a specific refinement, non-hydrogen atoms could be anchored through anisotropic displacement parameters. Through a riding model, the hydrogen atoms were determined. Then, the structure of MOF-1 was refined on F^2 using SHELXL-1997. According to the difference Fourier map, part of the coordinated DMA molecule, the guest $[(CH_3)_2NH_2]^+$ cation and lattice H_2O have been found, but they all suffered from severe disorganization. Therefore, using PLATON/SQUEEZE, a collection of solvent-free diffraction intensities is produced by removing the diffuse electron densities coming from these molecules. The larger *R* and w*R* values come from the fact that these guest species are not localized. This is where the category B warning on the checkcif report comes from. The CCDC number for MOF-1 is 2059712.

Results and discussion

Synthetic analysis

MOF-1 was self-assembled from the metal salt Cd^{2+} and the hexacarboxylic acid ligand H_6L in a mixed solvent (DMA : H_2O = 4 : 1). The temperature and pH of the reaction system and the choice of solvent play a key role in the formation of materials. Firstly, the temperature of the reaction system mainly affects the degree of crystallization of the material. MOF-1 can only be synthesized at 105 °C in order to obtain crystals suitable for single-crystal diffraction. A lower

 This journal is © The Royal Society of Chemistry 2024

Published on 23 July 2024. Downloaded on 11/19/2024 3:34:02 PM.

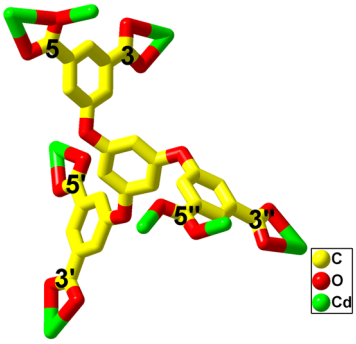

Fig. 1 Coordination modes of L^{6-} in MOF-1.

temperature obtains powders containing impurities, whereas a higher temperature is unfavorable due to the encapsulation of DMA in the pores. Secondly, the pH of the reaction system determines whether the target compounds can be obtained or not. MOF-1 can only be obtained at pH = 4, while under other pH conditions, part of the sample could not be synthesized and part of the synthesized sample was not pure. The reason may be that a strongly acidic environment is not conducive to the complete deprotonation of the carboxylic acid ligand H_6L, whereas a weakly acidic environment is not conducive to the formation of $[(CH_3)_2NH_2]^+$. Finally, DMA plays an important role. It not only acts as a neutral guest molecule to stabilize the framework, but also forms $[(CH_3)_2NH_2]^+$ to balance the charge of this anionic MOF during decarbonylation.

Structural description

X-ray single-crystal diffraction analysis reveals that MOF-1 is an L^{6-} extended 3-D Cd^{2+} anionic MOF. It crystallizes in the space group $P\bar{1}$, and in its asymmetric unit, only two Cd^{2+} centers and one L^{6-} anion are found. Cd1 is in a twisted pentagonal bipyramidal site, whereas Cd2 adopts an octahedral geometric configuration (Fig. S1a and S1b†). Both are surrounded by carboxyl O atoms with a slightly wide Cd–O distance ranging from 2.191(1) to 2.585(8) Å. L^{6-} exhibits a $\eta^1\eta^1\eta^1\eta^0\eta^1\eta^1\eta^1\eta^1\eta^1\eta^1\eta^1\eta^1:\mu_7$ coordination mode (Fig. 1).

As shown in Fig. 2d, the self-assembly between μ_7-mode L^{6-} and two types of Cd^{2+} forms a 3-D porous network. Firstly, μ_7-mode L^{6-} utilizes three carboxyl groups on 3,5 and 5′ positions to connect the Cd1 centers into a 1-D endless tube, extending along the *a*-axial direction (Fig. 2a). The size for tube opening is 1.45 nm × 0.86 nm. In Fig. 2a, the carboxyl group on the 3′ position is omitted. The fourth benzene ring in L^{6-} is also omitted. The carboxyl group on the 5 position also coordinates to another Cd^{2+} center (Cd2). The Cd2 centers like thorns are distributed on both sides of the tube. As exhibited in Fig. 2b, the fourth aromatic ring in L^{6-} appears. Two carboxyl groups (3″,5″ positions) on it

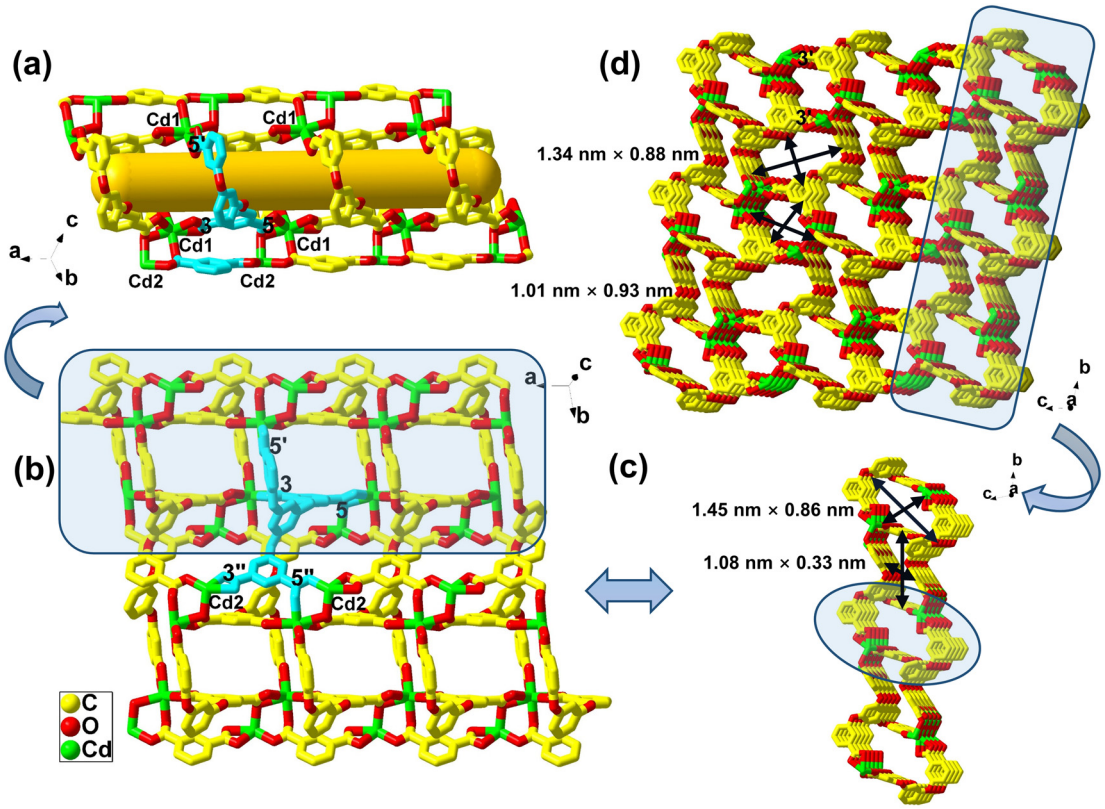

Fig. 2 1-D tube extending along the *a*-axial direction (a), 2-D layer (b and c) and projection diagram in the (100) direction (d) for MOF-1.

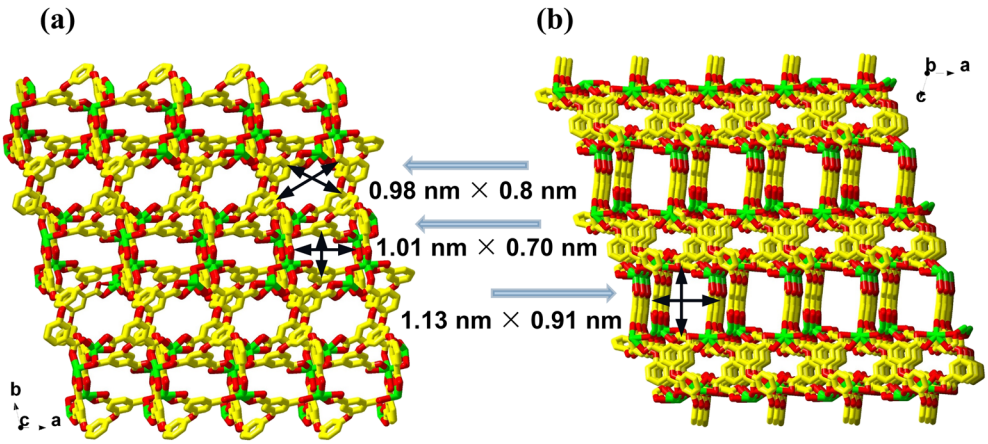

Fig. 3 Projection diagrams in (001) (a) and in (010) (b) directions for MOF-1.

Published on 23 July 2024. Downloaded on 11/19/2024 3:34:02 PM.

coordinate to two Cd2 centers from the neighboring tube. The benzene ring between two Cd2 centers in Fig. 2a comes from the adjacent tube. By this kind of interaction, the adjacent tubes are expanded into a 2-D layer. In the layer, a dinuclear $Cd_2O(COO)$ cluster is observed with a short Cd···Cd separation of 3.951 Å. Fig. 2c is the projection of the layer in the (100) direction. Between two neighboring tubes, a new tunnel is found. Unfortunately, this tunnel is too narrow, and the width is only 3.3 Å. In Fig. 2d, the 3′-position carboxyl group appears, and chelates to Cd2 from the neighboring layer. Through the interactions between this carboxyl group and Cd2, the adjacent layers interlock into the 3-D title porous network of MOF-1. In this process, two kinds of new tunnels are also formed, and the window for the larger channel is 1.34 nm × 0.88 nm. Since all of the carboxyl groups on L^{6-} are involved in coordination, it means that L^{6-} is in a fully deprotonated state, and its oxidation state in MOF-1 should be −6. According to element and TG analyses, there should also be three DMA molecules and two lattice water molecules in the asymmetric unit of MOF-1. As guests, these cations and molecules occupy the tunnel space, making MOF-1 more stable. In projection plots of (001) and (010) orientations, 1-D tunnels are also observed, and the window size has been marked on the images (Fig. 3a and b). The PLATON program reveals that the guest accessible void volume in MOF-1 is about 1639 $Å^3$. Considering charge equilibrium, there should be two $[(CH_3)_2NH_2]^+$ cations in the asymmetric unit of MOF-1.

Determination of the formula composition of MOF-1

According to the powder XRD patterns (Fig. 4), it can be seen that the diffraction peaks of the treated compound remain unchanged. The framework of MOF-1′ remains stable. The structure of MOF-1′ is well stabilized in solvent H_2O (MOF-1′-H_2O represents the powder sample of MOF-1′ stirred and soaked in deionised water and then dried.). Fig. S2a and S2b† show that MOF-1′ remains backbone stable in different solvents as well as in deionised water at pH = 3–11. It ensures its application in dye adsorption. Fig. S3† shows the thermogravimetric curve of MOF-1 in the temperature range of 40–800 °C under air atmosphere. MOF-1 undergoes a three-step sequential weight loss process. The first step of weight loss (*ca.* 2.9%) at 40–97 °C corresponds to the loss of two crystalline water molecules. The weight loss (*ca.* 21.5%) in the second step occurred at 97–202 °C, corresponding to the loss of three DMA molecules. The last step of weight loss (*ca.* 20.8%) occurs at 202–480 °C. The skeleton of MOF-1 collapses and its residue is finally identified as CdO. The above results are consistent with elemental analysis values of MOF-1, thus further confirming the accuracy of its molecular formula. Fig. S4† gives the IR spectrum of MOF-1.

Dye adsorption property

A number of factors can influence the final adsorption capacity in dye adsorption, including the adsorbent's specific surface area and pore size in terms of surface charge changes (caused by host–guest interactions like ion-ion exchange, D–A (donor–acceptor) interactions, π–π interactions, electrostatic interactions, hydrogen bonding, and van der Waals

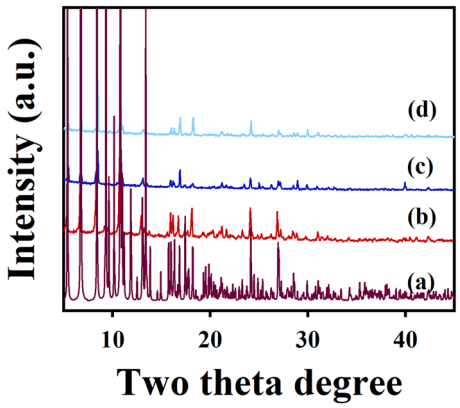

Fig. 4 Powder XRD patterns of simulated MOF-1 (a), experimental MOF-1 (b), MOF-1′ (c), and MOF-1′-H_2O (d).

 This journal is © The Royal Society of Chemistry 2024

Published on 23 July 2024. Downloaded on 11/19/2024 3:34:02 PM.

interactions).[41] The oxygen spacer group in L^{6-} of MOF-1 not only preserves the stability of the framework but also slightly distorts it to make it more conducive to dye entry into pores. Furthermore, lone electron pairs on oxygen atoms change the surface charge of MOF-1, facilitating dye adsorption.

Considering potential ion–ion exchange interactions, electrostatic interactions and D–A interactions between MOF-1 and cationic dyes, we selected five dyes of three types for adsorption experiments: rhodamine B (RB^+), methylene blue (MB^+), and azure A chloride (AA^+) for cationic dyes; bromocresol purple (BP) for neutral dye; and methyl orange (MO^-) for anionic dye. First, 10 mg MOF-1′ were respectively added to 40 ml dye aqueous solutions (10 mg L^{-1} for each kind of dye solution) to create five suspensions. Additionally, we compared photos of beginning and final colors following the addition of MOF-1′ to represent its adsorption and tracked variations in concentration of these suspensions over time using ultraviolet-visible (UV-vis) spectroscopy. After addition of MOF-1′ in photographs of Fig. 5, the color of MB^+ solution progressively turned colorless, the color of AA^+ solution became quite light and almost colorless, and the color of RB^+ solution slightly lightened, while the color of BP and MO^- solutions stayed the same. As shown in Fig. 5, within 480 min, the concentration of MB^+ almost decreased by *ca.* 95%, the concentration of AA^+ decreased by *ca.* 70%, and the concentration of RB^+ decreased by only *ca.* 42%, while the concentration of neutral dye BP and anionic dye MO^- was nearly unchanged. These results agree with observations that can be seen with unaided eye.

There are many reasons for the above phenomenon. After activation, guest molecules such as DMA and H_2O were removed, and the pores of MOF-1′ were revealed, so it could theoretically adsorb the five dyes. However, we found that MOF-1′ adsorbed cationic dyes significantly, while adsorption of neutral and anionic dyes was almost negligible. This may be due to the presence of a large number of $[(CH_3)_2NH_2]^+$ cations in the pores formed by decarbonylation of DMA in order to balance the backbone charge of MOF-1′. In the adsorption of dyes, these dimethylammonium cations can exchange with cationic dyes. The resulting driving force works well to make adsorption of the adsorbent more effective. In other words, the main driving force for adsorption of dyes by MOF-1 was ion exchange. Of course, the size of dye molecules and pores is also closely related to the adsorption effect. The literature indicates that the ideal ratio of the porous polymer material as an adsorbent to the adsorbent diameter is 2–6, and the adsorption effect is adversely affected by pore sizes that are either too large or too small.[42] Among these five dye molecules we chose, RB^+ (molecular size of RB^+ is optimized to be 1.44 nm × 1.09 nm × 0.64 nm)[43] and BP molecules are similar in size and both are larger than the other three dye molecules, the MO^- molecule (molecular sizes of MO^- is optimized to be 1.19 nm × 0.67 nm × 0.38 nm)[43] is in the middle size, and MB^+ (molecular sizes of MB^+ is optimized to be 1.19 nm × 0.67 nm × 0.38 nm)[38] and AA^+ molecules are similar in size and are the smallest molecules (Chart S2† is the molecular structure of five dyes). Meanwhile the largest pore size of

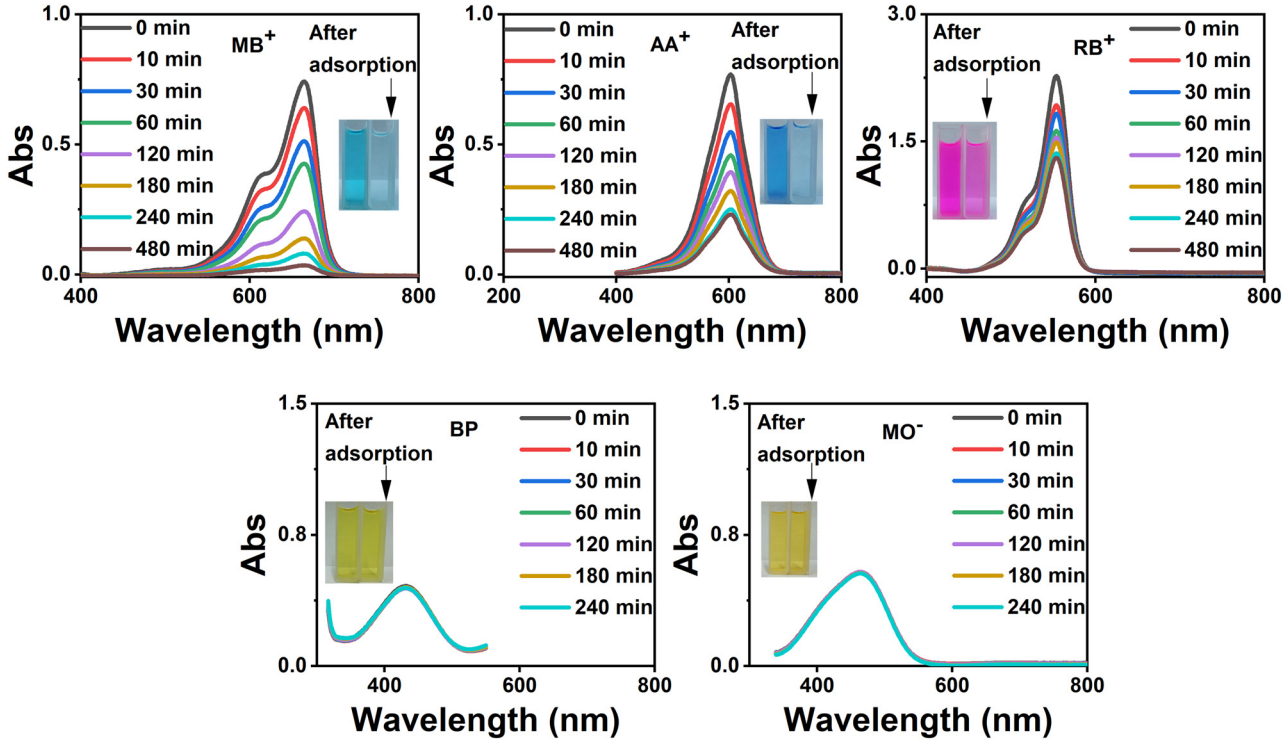

Fig. 5 Temporal evolution of UV-vis spectra absorption of 40 mL five dye solutions (10 mg L^{-1} for each kind of dye solution) after adding powder samples of MOF-1′ (10 mg). The photographs show the color of solutions before and after 240 or 480 min of dye adsorption.

Published on 23 July 2024. Downloaded on 11/19/2024 3:34:02 PM.

MOF-1 is 1.45 nm × 0.86 nm. In this regard, MOF-1′ is a suitable adsorbent for MB^+ and AA^+. This also explains why MOF-1' has a smaller adsorption capacity for RB^+ compared to MB^+ and AA^+.

To confirm the above adsorption mechanism speculation, we investigated whether MOF-1 has selectivity towards cationic dyes in mixed dyes. Furthermore, we need to take into account the situation that small molecules of cations firstly enter the pores of MOF-1, while larger molecules of neutral and anionic dyes cannot enter due to pore blockage. This seems to mislead to the assumption that MOF-1 is selective for the adsorption of cationic dyes. Therefore, we purposely chose the larger RB^+ molecule as a representative of cationic dyes, which was mixed with BP and MO^-. We tested the adsorption capacity of MOF-1′ (20 mg) in mixed dyes (80 ml, 5 mg L^{-1} for each kind of dye in solutions). UV-vis spectroscopy is used to detect changes in the concentration of dyes in solutions. In photographs of Fig. 6, after adding 20 mg MOF-1′ and after 24 h, the mixed solution of RB^+ and BP gradually changed from orange-red to yellowish green, and the mixed solution of RB^+ and MO^- gradually changed from orange-pink to orange. As shown in Fig. 6, the peak at 433 nm was attributed to BP, the peak at 566 nm was attributed to RB^+, and the peak at 466 nm was attributed to MO^-. After 24 h, the concentration of RB^+ in the mixed solution of RB^+ and MO^- decreased by *ca.* 74% (Fig. 6a), while the concentration of MO^- was almost unchanged. In the mixed solution of RB^+ and BP, the concentration of RB^+ decreased by *ca.* 77% (Fig. 6b), while the concentration of BP was almost unchanged. This indicates that even though RB^+ molecules are large, MOF-1′ still adsorbs cationic dyes rather than the smaller anionic or neutral dyes. It suggests that the size of the dye molecule does not influence the selectivity of dye adsorption by MOF-1′. This further confirms our conjecture that there is an ion-exchange driving force for dye adsorption of this anionic backbone material, MOF-1, which takes precedence over other forces.

Since there is a variability in adsorption of cations as observed in Fig. 5, in order to investigate whether the adsorption of cations by MOF-1 is selective, we investigated the adsorption behavior of MOF-1′ (10 mg) for two cationic mixed dye solutions (80 ml, 5 mg L^{-1} for each kind of dye in mixed solutions). As shown in Fig. 7a and c, the absorbance of cationic dyes decreased synchronously with time in each mixed solution. In terms of removal efficiency (removal efficiency = $(c_0 - c_t)/c_0 \times 100\%$, c_0 represents the original concentration and c_t represents the concentration at moment t) (Fig. 7b and d), the adsorption efficiencies of MB^+ and AA^+ were comparable, whereas the removal efficiency of cationic dyes with larger molecules was lower than that of smaller cationic dyes (MB^+ or AA^+). Overall, the size of dye molecules affects the adsorption rate of the adsorbent, with smaller dyes being adsorbed faster. MOF-1 is not selective for adsorption of cationic dyes. But we found that even though the molecular weight and structures of MB^+ and AA^+ are similar, MOF-1 has a larger and faster adsorption capacity for MB^+. This situation may be attributed to the different spatial positions of methylene groups on the two dye molecules, which resulted in different fitness to the pores of MOF-1′, and the molecular size of MB^+ was better fitted to the pores of MOF-1, so its adsorption was more complete.

To understand the adsorption behavior of MOF-1 and its mechanism, isotherm models play a crucial role as they provide information about the interaction between the adsorbent and adsorbate in any system. Taking MB^+ as an example, we tested the adsorption capacity of MOF-1′ to different concentrations of dye solutions (0, 10, 20, 40, 100, 200, 400, 800, and 1000 mg L^{-1}, respectively) at room temperature for the same time (one hour after adding 10 mg MOF-1′ to each different concentration of dye solutions). By connecting each point of adsorption equilibrium, we formed the adsorption curve in the shape of a type I (R^2 = 0.992) isotherm (Fig. 8). The maximum adsorption capacity (q_e) of MOF-1′ calculated from the Langmuir equation is 1378 mg g^{-1}. The adsorption isotherm curves were based on

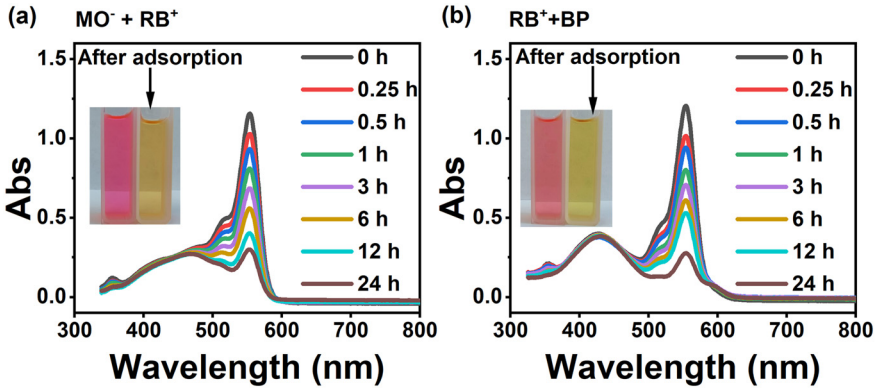

Fig. 6 Temporal evolution of UV-vis absorption spectra of 80 ml mixed dye solution ((a) MO^- + RB^+, (b) RB^+ + BP, 5 mg L^{-1} for each kind of dye in mixed solutions) after adding powder samples of MOF-1′ (20 mg). Photographs show the color of solutions before and after 24 h of dye adsorption.

 This journal is © The Royal Society of Chemistry 2024

Published on 23 July 2024. Downloaded on 11/19/2024 3:34:02 PM.

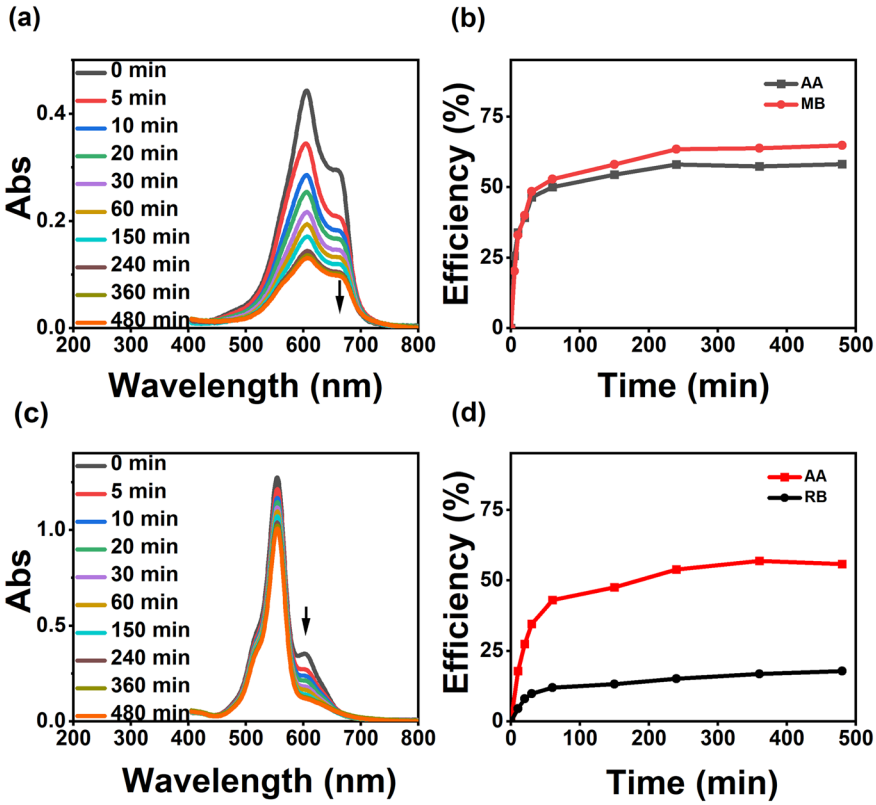

Fig. 7 Temporal evolution of UV-vis absorption spectra of 80 ml mixed dye solution ((a) MB^+ + AA^+, (c) RB^+ + AA^+, 5 mg L^{-1} for each kind of dye in mixed solutions) after adding powder samples of MOF-1′ (10 mg). Temporal evolution of removal efficiency of cationic mixed dye solutions ((b) MB^+ + AA^+, (d) RB^+ + AA^+) after adding powder samples of MOF-1′ (10 mg).

the Langmuir equation and plotted. The adsorption of dyes by MOF-1 consists of two parts: one is driven by ion exchange, and the other is due to the presence of certain surface adsorption.

At the same time, we investigated the maximum adsorption of MOF-1 for MB^+. 0.5–5 mg of MOF-1′ powder samples were put into the same plastic centrifuge tubes containing 1 mg MB^+ (40 mL, 25 mg g^{-1}) respectively. And according to Fig. 9, it can be seen that within 24 h, 1–5 mg MOF-1′ could completely adsorb 1 mg MB^+, while 0.5 mg MOF-1′ could not fully adsorb MB^+. Bringing into eqn (S1),†[44]

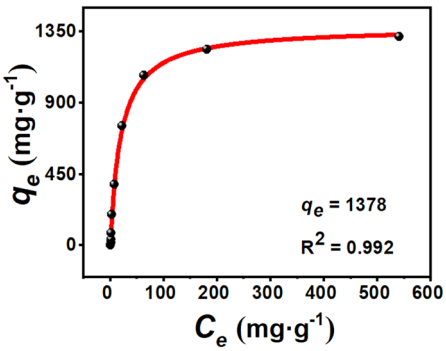

Fig. 8 Adsorption kinetics isotherm of MB^+ by MOF-1′ at room temperature.

based on the adsorption of 0.5 mg adsorbent for 1 mg dye, the maximum adsorption of MB^+ by MOF-1 was calculated to be *ca.* 1220 mg g^{-1}, which is similar to the 1378 mg g^{-1} mentioned above and higher than most of the reported adsorbents (Table S3†). Compared with other reported adsorbent materials, MOF-1 has a considerable adsorption capacity. This may be due to the role of oxygen active sites in channels. The D–A interaction between the chromophore group of dyes and the oxygen active site promotes the adsorption of MOF-1′. And the presence of oxygen spacer groups slightly regulates the pores and promotes the entry of dye molecules. In addition, electrostatic interactions may also exist and promote the adsorption of dyes. To investigate their interactions, we sonicated a 1 mg sample adsorbed with 1.2 mg of MB^+ and found that the solution would turn light blue, indicating that a part of the adsorbed MB^+ could be released during sonication. The adsorption of this part is generated by the D–A interactions. As shown in Fig. S5,† the absorbance of the fourth and fifth ultrasonic treatments almost overlaps, indicating that the ultrasonic treatment has been completed. According to the absorbance calculation from the UV spectrum, the adsorption capacity of MOF-1′-1 (10 mg MOF-1′ with 1200 mg MB^+) for MB^+ is *ca.* 270 mg due to the D–A interactions. In the maximum adsorption capacity of MOF-1′ for MB^+, it can be calculated that the

Published on 23 July 2024. Downloaded on 11/19/2024 3:34:02 PM.

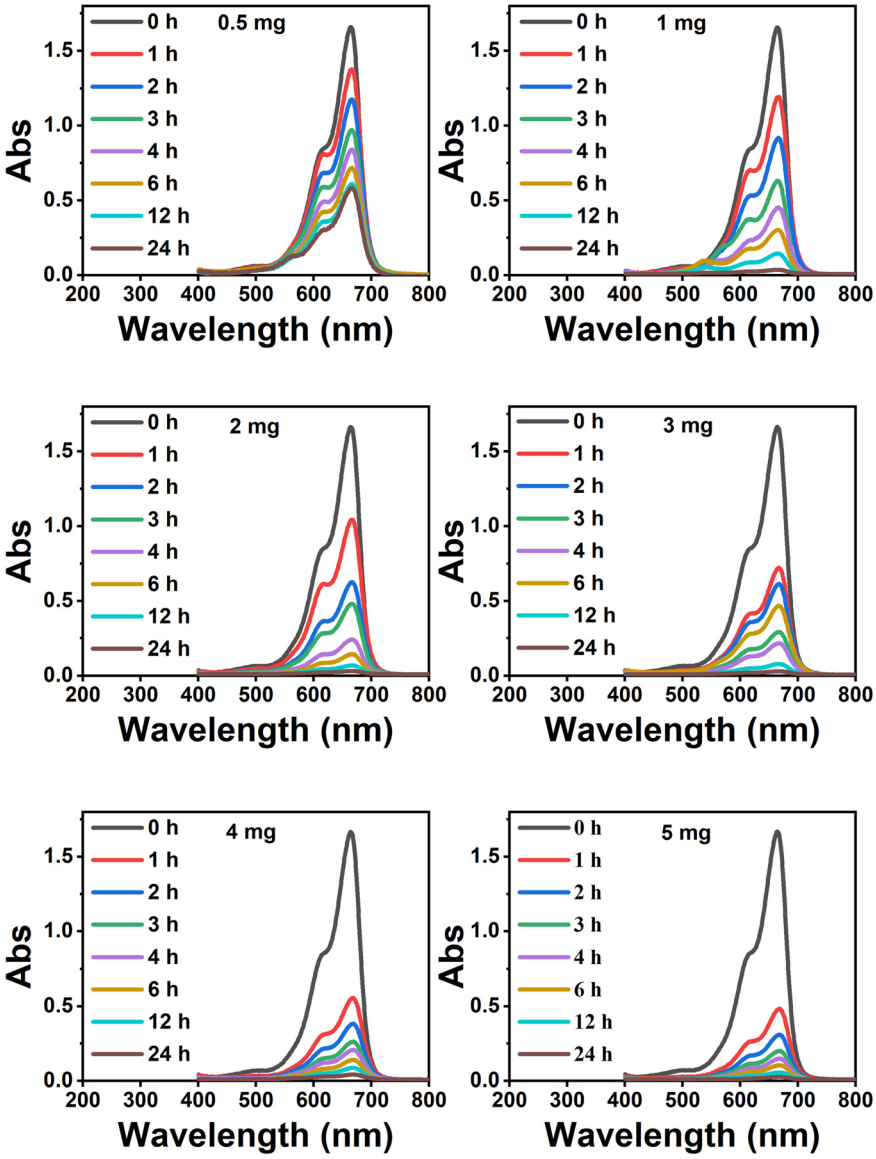

Fig. 9 Temporal evolution of UV-vis absorption spectra of 40 ml dye solution of MB^+ (40 mL, 25 mg L^{-1}) after adding powder samples of MOF-1′ (0.5–5 mg), respectively.

adsorption capacity generated by ion exchange is *ca.* 805 mg. The remaining adsorption amount may be caused by two reasons: one is that dyes in pores of MOF-1 were not completely sonicated during ultrasonic treatment, and the other is that adsorption may be caused by electrostatic interactions.

Compared with the previous work carried out by our group, we found that the adsorption capacity of anionic framework materials for cationic dyes is directly proportional to the molar ratio of cations and the compound, directly proportional to the molar mass of dye molecules, and inversely proportional to the molar mass of the compound. For examples, compound **1** ($[(CH_3)_2NH_2][Cd(L)\cdot DMA]\cdot 0.5DMA\cdot 1.5H_2O$) previously synthesized by Ding[38] in our group had a cation to compound ratio of 1 : 1, and its adsorption of the dye MB^+ by ion exchange was 540 mg g^{-1}; meanwhile the compound synthesized in this paper has a cation to compound ratio of 2 : 1 and the adsorption produced by ion exchange is 805 mg g^{-1}. Taking all factors into consideration, although the molar mass of dye molecules is directly proportional to the adsorption capacity of the compound, dyes with excessively large molecular diameters can lead to a decrease in adsorption capacity due to pore blockage. This is also why the cationic dye RB^+ with large molecules is relatively less adsorbed. This is another indication of the decisive and preferential role of the ion exchange driving force in the adsorption of cationic dyes by anionic MOFs.

To further investigate the adsorption capacity of MOF-1 for cationic dyes, we investigated its adsorption kinetics. According to the quasi-second order kinetic model, we quantified the adsorption rate by connecting the adsorption amount of each dye corresponding to each time point as

 This journal is © The Royal Society of Chemistry 2024

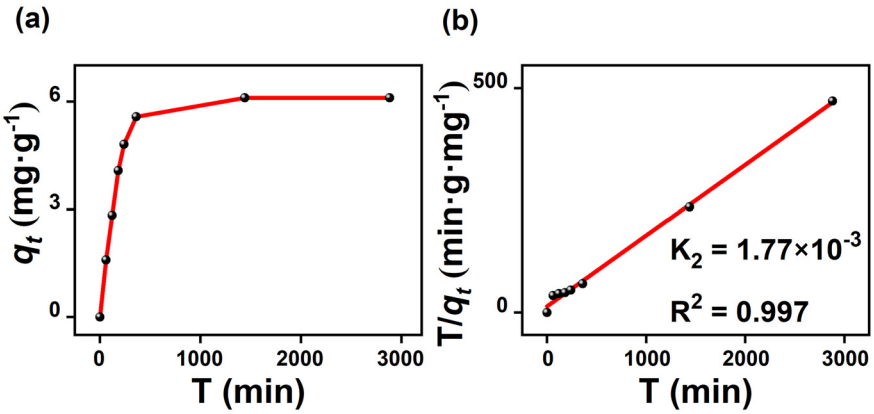

Fig. 10 Plot of variation of adsorption of MOF-1′ for MB^+ solution at different moments (a); plot of T/q_t. *Vs.* T of MOF-1′ on MB^+ solution at different moments (b).

Published on 23 July 2024. Downloaded on 11/19/2024 3:34:02 PM.

shown in eqn (S2).†[44] We obtained the q_t–T curve of MOF-1′ for MB^+ (Fig. 10a). The T/q_t *vs.* T curve was plotted and fitted (Fig. 10b). The R^2 value of the curve was 0.997 and the adsorption rate constant was 1.77×10^{-3} g mg^{-1} min^{-1}, which showed that MOF-1′ adsorbed MB^+ faster compared to the adsorption rate of other materials (Table S4†).[45–51]

An important indicator for the stability of a good adsorbent is recyclability. We first attempted to test the desorption behavior of MOF-1′ on MB^+. In order to avoid potential charge imbalance and skeleton collapse that may result from dye desorption, we chose saturated NaCl acetonitrile solution and pure acetonitrile solution (40 mL each) to investigate the desorption behaviour of MOF-1′ for the cationic dye MB^+. MOF-1′-1 (loaded with 1 mg MB^+) was added to the above solution. As shown in Fig. S6a,† the concentration of dye in the saturated NaCl solution increased with time until it no longer increased and was similar to the initial concentration, which indicated that the adsorbed MOF-1′ had already desorbed MB^+, and MB^+ was almost completely desorbed after 12 h. As a comparison, a desorption experiment was also performed in a pure CH_3CN solution. As shown in Fig. S6b,† the UV-vis absorption intensity of dye solution remains constant with time. This indicates that the desorption process did not occur. These results suggest that MOF-1′-1 releases MB^+ through ion exchange between Na^+ and MB^+.

Next, cyclic adsorption–desorption experiments of MOF-1′ on MB^+ were performed. As shown in Fig. 11, adsorption–desorption cycling experiments between MOF-1′ and MB^+ were performed under the same conditions each time and could be carried out for at least five cycles without loss of absorptive capacity of MOF-1′. After the fifth adsorption, its adsorption efficiency decreased to *ca.* 85%, while after the fifth desorption, its desorption efficiency decreased to *ca.* 70%. As shown in Fig. S7,† the XRD characterization confirmed that MOF-1′ was stable after one cycle to five cycles of adsorption and desorption. The above dye adsorption experiments proved that MOF-1 is a good anionic skeleton material, which can have an excellent adsorption performance for cationic MB^+. And MOF-1 has good stability and can be recycled more than 5 times.

Based on the above experimental results, we can deduce the relationship between the pore structure of MOF-1 and adsorption properties of the material, and explain the adsorption mechanism of MOF-1 for dyes:

1. MOF-1 effectively adsorbs cationic dyes and the driving force is mainly ion exchange.

2. The main factors affecting the adsorption efficiency and maximum adsorption capacity are as follows: (i) the pore size of MOFs directly affects the adsorption properties of the materials. The windows of pores need to be large enough to accommodate the entry of dye molecules from one side or the other, and the size exclusion effect of pores affects the final adsorption of small molecule cationic dyes. (ii) For forces involved in the adsorption process, the decisive factor is ion exchange. The strength and maximum theoretical capacity of this force can be known by calculation, which is proportional to the proportion of cations in the compound. The ratio is decisive among these factors. (iii) The effective proximity to the solvent volume of this type of compound in the dye adsorption process has an effect on adsorption performance. Cationic guest molecules involved in ion exchange are not affected, but neutral or anionic guest molecules that are not removed during the activation process can cause clogging of the pores, which reduces the effective capacity of the compound's pores, resulting in a decrease in the maximum adsorption capacity and a slowing down of adsorption rate. Although the compound previously synthesised by our group[38] had a solvent accessible volume of about 4000 Å^3, the large proportion of DMF guest molecules in the compound reduced its effective pore space, so the maximum adsorption capacity was only about 900 mg g^{-1}. (iv) The introduction of oxygen spacer groups not only resulted in enhanced stability of MOF-1's structure, but also improved the adsorption properties of MOF-1 to MB^+ through D–A interaction with the dye.

Published on 23 July 2024. Downloaded on 11/19/2024 3:34:02 PM.

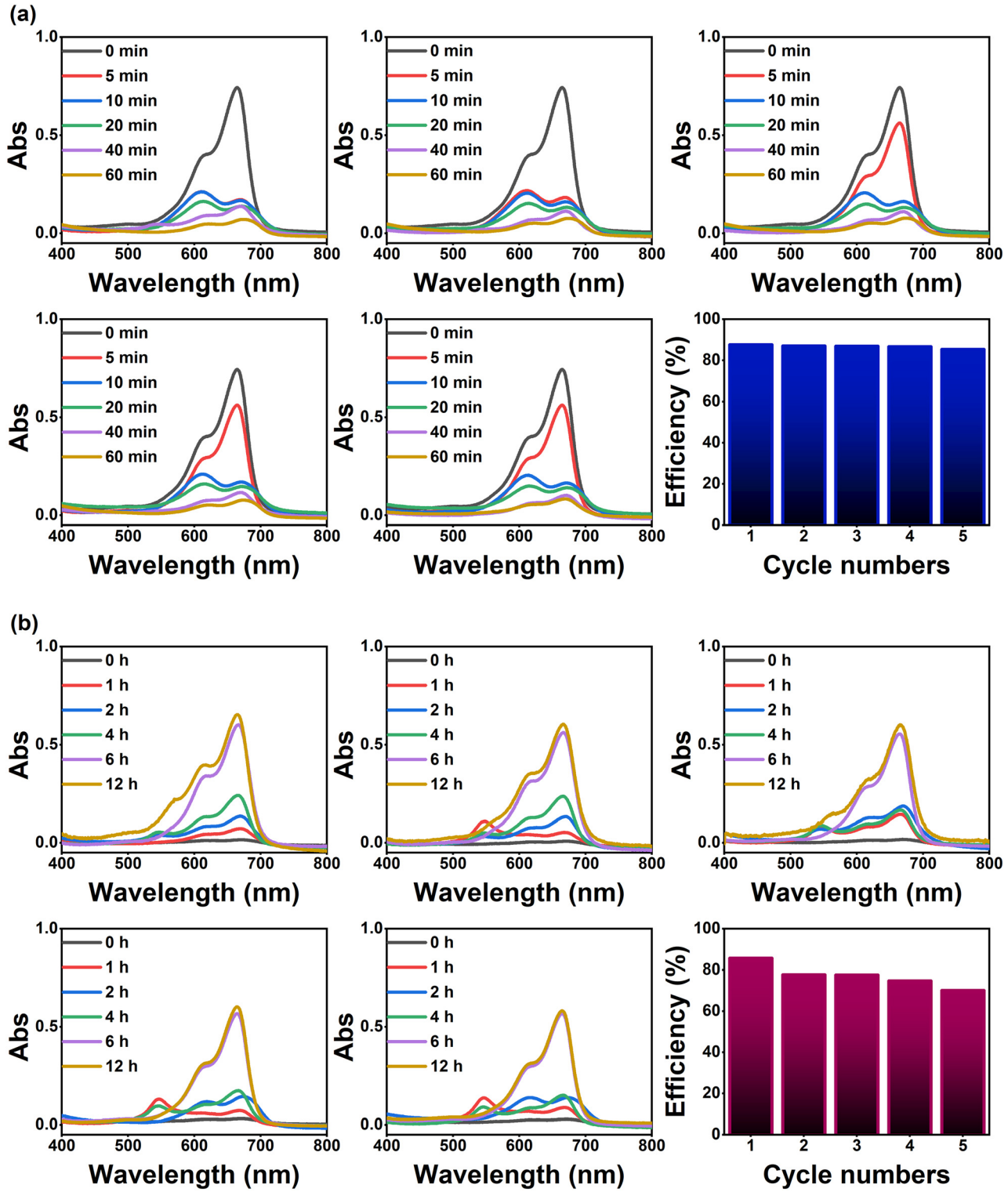

Fig. 11 Five runs of recycling and efficiency for adsorption (a) and desorption (b) experiments of MB^+ by MOF-1′.

Conclusion

In conclusion, we successfully synthesized a unique polycarboxylic acid based 3-D anionic MOF (MOF-1), which showed good thermal and chemical stability. After activation to remove solvent molecules from backbone pores, the potential guest and void volume of MOF-1' is about 1639 $Å^3$. Tetragonal-like pores and abundant oxygen vacancies in the skeleton enhance the ability of adsorption and separation of dyes. Meanwhile, MOF-1 could selectively adsorb cationic

 This journal is © The Royal Society of Chemistry 2024

Published on 23 July 2024. Downloaded on 11/19/2024 3:34:02 PM.

dyes of appropriate sizes and shapes in aqueous solution through an ion-ion exchange process and exhibited a record high adsorption capacity (1220 mg g^{-1}) for MB^+. The amount of adsorption due to ion exchange is 805 mg. Ion exchange is the main driving force for adsorption of cationic dyes by MOF-1 and is preferred over other forces. And in the saturated NaCl solution of CH_3CN, the adsorbed dyes were released from the framework again, and MOF-1 was recycled with good efficiency and stability.

Data availability

The data supporting this article have been included as part of the ESI.† Crystallographic data for MOF-1 has been deposited at the CCDC under 2059712.

Author contributions

The manuscript was written through contributions of all authors. All authors have given approval to the final version of the manuscript. Yuxuan Xiong: conceptualization, methodology, validation, investigation, data curation, writing – original draft, writing – review & editing, visualization. Dan-Dan, Li: methodology, writing – review & editing. Jie-Hui Yu: conceptualization, methodology, writing – review & editing, supervision, project administration. Qingfeng Yang: conceptualization, methodology, writing – review & editing.

Conflicts of interest

The authors declare no competing financial interest.

Acknowledgements

The authors are grateful for the financial aid from the National Natural Science Foundation of China (Grant No. 21771076).

References

1 P. M. D. S. Silva, T. R. Fiaschitello, R. S. d. Queiroz, H. S. Freeman, S. A. d. Costa, P. Leo, A. F. Montemor and S. M. d. Costa, Natural Dye from Croton Urucurana Baill. Bark: Extraction, Physicochemical Characterization, Textile Dyeing and Color Fastness Properties, *Dyes Pigm.*, 2020, **173**, 107953.
2 A. K. Smith, Health Hazards of the Dye Industry, *Am. J. Public Health*, 1920, **10**(3), 255–257.
3 M. Mahbubul Bashar and M. A. Khan, An Overview on Surface Modification of Cotton Fiber for Apparel Use, *J. Polym. Environ.*, 2012, **21**(1), 181–190.
4 R. Molinari, C. Lavorato and P. Argurio, Recent Progress of Photocatalytic Membrane Reactors in Water Treatment and in Synthesis of Organic Compounds. A review, *Catal. Today*, 2017, **281**, 144–164.
5 I. Safarik, S. Mullerova and K. Pospiskova, Magnetic Textile Solid Phase Extraction of Cationic Dyes from Water Solutions, *Fibers Polym.*, 2020, **21**(12), 2836–2841.
6 T. Tomić, S. Babić, M. Biošić, N. U. Nasipak and A.-M. Čižmek, Determination of the Solvent Blue 35 Dye in Diesel Fuel by Solid Phase Extraction and High-Performance Liquid Chromatography with Ultraviolet Detection, *Dyes Pigm.*, 2018, **150**, 216–222.
7 M. Sadeghi, M. Heydari and V. Javanbakht, Photocatalytic and Photo-Fenton Processes by Magnetic Nanophotocatalysts for Efficient Dye Removal, *J. Mater. Sci.: Mater. Electron.*, 2021, **32**(4), 5065–5081.
8 N. N. Bahrudin, M. A. Nawi and Z. Zainal, Insight Into the Synergistic Photocatalytic-Adsorptive Removal of Methyl Orange Dye Using TiO_2/Chitosan Based Photocatalyst, *Int. J. Biol. Macromol.*, 2020, **165**, 2462–2474.
9 A. Sandoval, C. Hernández-Ventura and T. E. Klimova, Titanate Nanotubes for Removal of Methylene Blue Dye by Combined Adsorption and Photocatalysis, *Fuel*, 2017, **198**, 22–30.
10 J. Zhang, H. Yu, X. Quan, S. Chen and Y. Zhang, Ceramic Membrane Separation Coupled with Catalytic Ozonation for Tertiary Treatment of Dyestuff astewater in a Pilot-Scale Study, *Chem. Eng. J.*, 2016, **301**, 19–26.
11 N. Baig, J. Usman, S. I. Abba, M. Benaafi and I. H. Aljundi, Fractionation of Dyes/Salts Using Loose Nanofiltration Membranes: Insight from Machine Learning Prediction, *J. Cleaner Prod.*, 2023, **418**, 138193.
12 J. Zhang, H. Tong, W. Pei, W. Liu, F. Shi, Y. Li and Y. Huo, Integrated Photocatalysis-Adsorption-Membrane Separation in Rotating Reactor for Synergistic Removal of RhB, *Chemosphere*, 2021, **270**, 270124.
13 M. C. Villalobos, A. A. P. Cid and A. M. H. González, Removal of Textile Dyes and Metallic Ions Using Polyelectrolytes and Macroelectrolytes Containing Sulfonic Acid Groups, *J. Environ. Manage.*, 2016, **177**, 65–73.
14 C. Peng, L. Chen, X. Wu, X. Wei, A. Tehrim, M. Dai and S. Xu, Identification of Adsorption or Degradation Mechanism for the Removal of Different Ionic dyes with Iron-Carbon Micro-Electrolysis Process, *J. Environ. Chem. Eng.*, 2021, **9**(4), 105690.
15 L. Cai, D. Ying, X. Liang, M. Zhu, X. Lin, Q. Xu, Z. Cai, X. Xu and L. Zhang, A Novel Cationic Polyelectrolyte Microsphere for Ultrafast and Ultra-Efficient Removal of Heavy Metal Ions and Dyes, *Chem. Eng. J.*, 2021, **410**, 128404.
16 N. A. Rosli, M. A. Ahmad, T. U. Noh and N. A. Ahmad, Pineapple Peel–Derived Carbon for Adsorptive Removal of Dyes, *Mater. Chem. Phys.*, 2023, **306**, 128094.
17 A. Ayati, M. N. Shahrak, B. Tanhaei and M. Sillanpää, Emerging Adsorptive Removal of Azo Dye by Metal–Organic Frameworks, *Chemosphere*, 2016, **160**, 30–44.
18 N. Akter, M. A. Hossain, M. J. Hassan, M. K. Amin, M. Elias, M. M. Rahman, A. M. Asiri, I. A. Siddiquey and M. A. Hasnat, Amine Modified Tannin Gel for Adsorptive Removal of Brilliant Green Dye, *J. Environ. Chem. Eng.*, 2016, **4**(1), 1231–1241.
19 M. A. Salam, S. A. Kosa and A. A. Al-Beladi, Application of Nanoclay for the Adsorptive Removal of Orange G Gye from Aqueous Solution, *J. Mol. Liq.*, 2017, **241**, 469–477.

Published on 23 July 2024. Downloaded on 11/19/2024 3:34:02 PM.

20 S. S. Batool, Z. Imran, S. Hassan, K. Rasool, M. Ahmad and M. A. Rafiq, Enhanced Adsorptive Removal of Toxic Dyes Using SiO_2 Nanofibers, *Solid State Sci.*, 2016, **55**, 13–20.
21 P. Srivatsav, B. S. Bhargav, V. Shanmugasundaram, J. Arun, K. P. Gopinath and A. Bhatnagar, Biochar as an Eco-Friendly and Economical Adsorbent for the Removal of Colorants (Dyes) from Aqueous Environment: A Review, *Water*, 2020, **12**(12), 3561.
22 M. U. Rehman, M. B. Taj and S. A. C. Carabineiro, Biogenic Adsorbents for Removal of Drugs and Dyes: A Comprehensive Review on Properties, Modification and Applications, *Chemosphere*, 2023, **338**, 139477.
23 T. H. Bui, C. Kim, S. P. Hong and J. Yoon, Effective Adsorbent for Arsenic Removal: Core/Shell Structural Nano Zero-Valent Iron/Manganese Oxide, *Environ. Sci. Pollut. Res.*, 2017, **24**(31), 24235–24242.
24 C.-T. Yu, H.-M. Lin and H.-W. Cheng, Synthesis of Mercury Sorbent Including Metal Oxides With Layered Carbonates Material, *Chem. Eng. J.*, 2015, **277**, 79–85.
25 R. Gusain, N. Kumar and S. S. Ray, Recent Advances in Carbon Nanomaterial-Based Adsorbents for Water Purification, *Coord. Chem. Rev.*, 2020, **405**, 213111.
26 O. M. Yaghi, G. Li and H. Li, Selective Binding and Removal of gGuests in a Microporous Metal–Organic Framework, *Nature*, 1995, **378**(6558), 703–706.
27 X. Liu, B. Tang, J. Long, W. Zhang, X. Liu and Z. Mirza, The Development of MOFs-Based Nanomaterials in Heterogeneous Organocatalysis, *Sci. Bull.*, 2018, **63**(8), 502–524.
28 P. Zhou, J. Lv, X. Huang, Y. Lu and G. Wang, Strategies for Enhancing the Catalytic Activity and Electronic Conductivity of MOFs-Based Electrocatalysts, *Coord. Chem. Rev.*, 2023, **478**, 214969.
29 L. Shen, G. Wang, X. Zheng, Y. Cao, Y. Guo, K. Lin and L. Jiang, Tuning the Growth of Cu-MOFs for Efficient Catalytic Hydrolysis of Carbonyl Sulfide, *Chin. J. Catal.*, 2017, **38**(8), 1373–1381.
30 Z. Zhao, M. A. Shehzad, B. Wu, X. Wang, A. Yasmin, Y. Zhu, X. Wang, Y. He, L. Ge and X. Li, *et al.*, Spray-Deposited Thin-Film Composite MOFs Membranes for Dyes Removal, *J. Membr. Sci.*, 2021, **635**, 119475.
31 D. Jiang, M. Chen, H. Wang, G. Zeng, D. Huang, M. Cheng, Y. Liu, W. Xue and Z. Wang, The Application of Different Typological and Structural MOFs-Based Materials for the Dyes Adsorption, *Coord. Chem. Rev.*, 2019, **380**, 471–483.
32 L. Yang, Y.-L. Liu, C.-G. Liu, F. Ye and Y. Fu, Two Luminescent Dye@MOFs Systems as Dual-Emitting Platforms for Efficient Pesticides Detection, *J. Hazard. Mater.*, 2020, **381**, 120966.
33 X. Zhao, M. Zheng, X. Gao, J. Zhang, E. Wang and Z. Gao, The Application of MOFs-Based Materials for Antibacterials Adsorption, *Coord. Chem. Rev.*, 2021, **440**, 213970.
34 F. Ma, Y. Gui, P. Liu, Y. Xue and W. Song, Functional Fibrous Materials-Based Adsorbents for Uranium Adsorption and Environmental Remediation, *Chem. Eng. J.*, 2020, **390**, 124597.
35 W. Qu, C. Chen, Z. Tang, H. Wen, L. Hu, D. Xia, S. Tian, H. Zhao, C. He and D. Shu, Progress in Metal-Organic-Framework-Based Single-Atom Catalysts for Environmental Remediation, *Coord. Chem. Rev.*, 2023, **474**, 214855.
36 D. Sun, Y. Ke, D. J. Collins, G. A. Lorigan and H.-C. Zhou, Construction of Robust Open Metal–Organic Frameworks with Chiral Channels and Permanent Porosity, *Inorg. Chem.*, 2007, **46**(7), 2725–2734.
37 F. Temesgen, N. Gabbiye and O. Sahu, Biosorption of Reactive Red Dye (RRD) on Activated Surface of Banana and Orange Peels: Economical Alternative for Textile Effluent, *Surf. Interfaces*, 2018, **12**, 151–159.
38 R. D. Ding, D. D. Li, F. Leng, J. H. Yu, M. J. Jia and J. Q. Xu, A Metal–Organic Framework with Rich Accessible Nitrogen Sites for Rapid Dye Adsorption and Highly Efficient Dehydrogenation of Formic Acid, *Dalton Trans.*, 2022, **51**(22), 8695–8704.
39 Y. Wang, M. He, X. Gao, S. Li, S. Xiong, R. Krishna and Y. He, Exploring the Effect of Ligand-Originated MOF Isomerism and Methoxy Group Functionalization on Selective Acetylene/Methane and Carbon Dioxide/Methane Adsorption Properties in Two NbO-Type MOFs, *ACS Appl. Mater. Interfaces*, 2018, **10**(24), 20559–20568.
40 D. Bai, Y. Wang, M. He, X. Gao and Y. He, Structural Diversities and Gas Adsorption Properties of a Family of Rod-Packing Lanthanide–Organic Frameworks Based on Cyclotriphosphazene-Functionalized Hexacarboxylate Derivatives, *Inorg. Chem. Front.*, 2018, **5**(9), 2227–2237.
41 J. Lu, Y. Zhou and Y. Zhou, Recent Advance in Enhanced Adsorption of Ionic Dyes from Aqueous Solution: A review, *Crit. Rev. Environ. Sci. Technol.*, 2023, **53**(19), 1709–1730.
42 J. A. Koehler, K. K. Wallace, P. J. Smith and G. F. Payne, Selective Adsorption of Sterically Hindered Phenols Through a Single-Point Binding Mechanism, *Ind. Eng. Chem. Res.*, 1999, **38**(8), 3076–3082.
43 J. H. Huang, K. L. Huang, S.-Q. Liu, A. T. Wang and C. Yan, Adsorption of Rhodamine B and Methyl Orange on a Hypercrosslinked Polymeric Adsorbent in Aqueous Solution, *Colloids Surf., A*, 2008, **330**(1), 55–61.
44 R. D. Ding, D. D. Li, J. H. Yu, M. J. Jia and J. Q. Xu, Porous 3,4-di(3,5-dicarboxyphenyl)hthalate-Based Cd^{2+} Coordination Polymer and Its Potential Applications, *Spectrochim. Acta, Part A*, 2021, **252**, 119498.
45 R. Lu, C. Wang, Y. Chen, L. Tan, P. Wang and S. Feng, IL-Unctionalized Mn(ii)-Doped Core–Shell Fe_3O_4@Zr-MOF Nanomaterials for the Removal of MB from Wastewater Based on Dual Adsorption/Fenton Catalysis, *New J. Chem.*, 2022, **46**(18), 8534–8544.
46 B. N. Li, X. L. Zhang, X. H. Bai, Z. J. Liang, J. Li and X.-Y. Fan, Electron-Rich Triazine-Conjugated Microporous Polymers for the Removal of Dyes from Wastewater, *Molecules*, 2023, **28**(12), 4785.
47 G. L. Gao, P. J. Zhou, C. Q. Chen and L. L. Zhu, Adsorption of MB and Pb(II) before and after Magnetic Modification: Performance and Mechanism, *J. Mol. Struct.*, 2023, **1293**, 139306.

 This journal is © The Royal Society of Chemistry 2024

48 X. Q. Qiao, F. C. Hu, F. Y. Tian, D. F. Hou and D. S. Li, Equilibrium and Kinetic Studies on MB Adsorption by Ultrathin 2D MoS_2 Nanosheets, *RSC Adv.*, 2016, **6**(14), 11631–11636.

49 J. Song, L. Chen, Y. Niu, Z. Wei and Y. Sun, Study on Amino-Functionalized Porous Carbon Materials for MB and Cr(VI) Adsorption, *J. Polym. Environ.*, 2023, **31**(7), 2999–3014.

50 Q. Fu and Y. Wu, Adsorption Behavior and Mechanism of Action of Magnetic MIL-100(Fe) on MB, *Environ. Monit. Assess.*, 2023, **195**(6), 745.

51 R. Li, X. Ren, J. Zhao, X. Feng, X. Jiang, X. Fan, Z. Lin, X. Li, C. Hu and B. Wang, Polyoxometallates Trapped in a Zeolitic Imidazolate Framework Leading to High Uptake and Selectivity of Bioactive Molecules, *J. Mater. Chem. A*, 2014, **2**(7), 2168–2173.

Published on 23 July 2024. Downloaded on 11/19/2024 3:34:02 PM.